Inference of the magnetospheric plasma mass density from field line resonances: A test using a plasmasphere model

M. Vellante[1] and M. Förster[2]

Received 23 December 2005; revised 11 August 2006; accepted 23 August 2006; published 1 November 2006.

[1] Using field-aligned ion density profiles from a physical-numerical model of the plasmasphere, we investigated the reliability of techniques which use field line resonance measurements to remotely sense the plasmaspheric mass density ρ, over $L = 1.6–3.4$. We find that the common assumption of some functional law for the variation of ρ along different field lines may lead to distorted profiles of the equatorial density ρ_o as inferred from the observed fundamental field line eigenfrequency. The tests show that for midlatitude field lines ($2.3 < L < 3.4$) a radial power law with an index $m \cong 1$ might be appropriate for a large variety of solar and geomagnetic conditions, and this index well represents the mass density dependence on the outer part of the field line. Indeed, an accurate integral expression of the field line eigenperiod demonstrates that the low-altitude plasma tube provides a negligible contribution to the eigenperiod. However, at lower latitudes, higher m values are necessary to obtain correct estimates of ρ_o. In this case m represents only an average index, not related to any particular variation of ρ along the field line. This effective index is also significantly dependent on solar activity conditions and local time. It turns out that inferred temporal variations of ρ_o at a given low L-shell can be significantly overestimated when a fixed functional dependence for the field-aligned mass density is assumed. The performance of more sophisticated techniques which use higher harmonics is also examined.

Citation: Vellante, M., and M. Förster (2006), Inference of the magnetospheric plasma mass density from field line resonances: A test using a plasmasphere model, *J. Geophys. Res.*, *111*, A11204, doi:10.1029/2005JA011588.

1. Introduction

[2] During the last few years it has become more and more popular to use ground-based ULF magnetic measurements to remote sense the plasma mass density in the magnetosphere [*Menk et al.*, 1999; *Chi et al.*, 2000; *Clilverd et al.*, 2003; *Berube et al.*, 2005]. The method consists in determining from ground observations the eigenfrequencies of the standing oscillations of a given geomagnetic field line and to deduce from them the plasma mass density (usually at the equatorial point of the given field line). Accurate determinations of the eigenfrequencies are made using the so-called "gradient method" [*Baransky et al.*, 1985] or the "cross-phase method" [*Waters et al.*, 1991]. These methods evaluate the eigenfrequencies (hereafter also referred to as resonant frequencies f_R) of the field line approximately midway between two recording stations closely separated in latitude (1–3 degrees). More sophisticated methods [*Kawano et al.*, 2002] can provide a continuous latitudinal profile of f_R within the field of view of the ground stations.

[3] Usually, the density inference is made by using only the fundamental eigenfrequency, which is more easily identified than the other harmonics. The standard procedure for inferring the equatorial plasma mass density ρ_o for low-latitude and midlatitude field lines assumes that the observed resonant frequency corresponds to an eigenfrequency of the axisymmetric toroidal Alfvén mode in a dipole field. The governing wave equation of this mode is the following [*Poulter et al.*, 1984]:

$$\frac{d^2\varepsilon(z)}{dz^2} + \lambda\left(1 - z^2\right)^6 \frac{\rho(z)}{\rho_o}\varepsilon(z) = 0 \qquad (1)$$

where $z = \cos\theta$ specifies the position along the field line, θ being the geomagnetic colatitude; $\varepsilon(z) = h_v(z)\, E_v(z)$, $E_v(z)$ being the electric wave field in the direction of the principal normal to the field line, and $h_v(z)$ being a dipole metric function; $\rho(z)$ is the plasma mass density along the field line. For each eigenvalue λ, the corresponding eigenfrequency f_R is given by:

$$f_R = \frac{B_E}{2\pi R_E \mu_o^{1/2}} \frac{\lambda^{1/2}}{L^4 \rho_o^{1/2}} = C \frac{\lambda^{1/2}}{L^4 \rho_o^{1/2}} \qquad (2)$$

where B_E is the equatorial value of the Earth's magnetic field at ground level, R_E the Earth's radius, μ_o the magnetic permeability of free space, and $L = r_o/R_E$ is the field line

[1]Dipartimento di Fisica, Università dell'Aquila, L'Aquila, Italy.
[2]GeoForschungsZentrum, Potsdam, Germany.

0148-0227/06/2005JA011588

Table 1. Summary of Power Law Density Indices Adopted in Papers Using Field Line Resonances to Remote Sense the Magnetospheric Plasma Mass Density

m	L	Reference
4	~7	*Waters et al.* [1995]
4	5–12	*Waters et al.* [1996]
4	5–12	*Loto'aniu et al.* [1999]
3	2.5–4.5	*Menk et al.* [1999]
3	1.9–2.2	*Russell et al.* [1999]
4	2	*Chi et al.* [2000]
3	1.7	*Berube et al.* [2003]
3	2.3–5.5	*Clilverd et al.* [2003]
3	2.7–5.8	*Dent et al.* [2003]
3–4	2.6–10	*Menk et al.* [2004]
3	1.7–3.1	*Berube et al.* [2005]
0	2.5–9	*Chi et al.* [2005]

distance in the equatorial plane in units of the Earth's radius. If we express the density in [amu/cm^3] and the frequency in [mHz], the numerical value of the constant C is $\sim 1.7 \times 10^4$. The eigenvalues are found imposing the boundary condition $\varepsilon = 0$ at $z = \pm z_i$, where the field line meets the ionosphere and the wave is reflected. In order to solve equation (1) it is necessary to assume a given functional form for the plasma mass density along the field line. The common assumption is a radial power law dependence:

$$\rho(r) = \rho_o (r/r_o)^{-m} \tag{3}$$

where $r = r_o \sin^2\theta = r_o (1 - z^2)$ is the geocentric distance along the field line.

[4] For any given L-shell and m value, the inferred equatorial density is found by inverting (2):

$$\tilde{\rho}_o \left[\text{amu/cm}^3\right] = \frac{K\lambda(L,m)}{L^8 f_R^2[\text{mHz}]} = \frac{A(L,m)}{f_R^2[\text{mHz}]} \tag{4}$$

where $K = C^2 \cong 3 \times 10^8$.

[5] Mainly because of its simplicity, the radial power law (3) has been the only functional dependence considered so far. Table 1 shows the values of the power law index m adopted in different papers. As can be seen, $m = 3$–4 represents the typical choice regardless of the L value. This choice mostly comes from past whistler observations of the radial dependence of the equatorial electron density [*Carpenter and Smith*, 1964]. More recently, it has been found that the radial dependence of the plasma mass density along the field lines is much slower than across the field lines. In particular, *Takahashi et al.* [2004] found that the relationship among the first three harmonics of the standing toroidal Alfvén waves observed by the CRRES satellite in the range $4 < L < 6$ were consistent with a power law index $m \sim 0.5$. Plasma wave data from the Polar spacecraft [*Goldstein et al.*, 2001; *Denton et al.*, 2002], radio sounding measurements from the IMAGE satellite [*Reinisch et al.*, 2001; *Huang et al.*, 2004], and measurements from the Retarding Ion Mass Spectrometer on the Dynamic Explorer 1 satellite [*Gallagher et al.*, 2000] all exhibit very small variations of electron and ion concentrations along plasmaspheric field lines for a significant length around the equator. Following these observations, *Chi et al.* [2005] preferred to adopt $m = 0$.

[6] In any case, it is generally considered that the derived equatorial density is only slightly dependent on m and that the deviation resulting from different choices is smaller than that arising from the error in the f_R estimate. These errors may have different sources: spectral method [*Kawano et al.*, 2002; *Berube et al.*, 2003], incorrect boundary conditions [*Allan and Knox*, 1979; *Yumoto et al.*, 1995; *Ozeke and Mann*, 2005], poloidal-toroidal mode coupling [*McClay*, 1970], spatial integration [*Hughes and Southwood*, 1976; *Poulter and Allan*, 1985], etc. Typical errors associated to the derived mass density, as resulting from the uncertainty in identifying f_R using the cross-phase technique, are 20–30% at $L > 2$ [*Clilverd et al.*, 2003; *Dent et al.*, 2003]. At lower L, because of the higher f_R values, the experimental relative error is generally lower. For instance, a typical error of 2 mHz associated to an f_R estimate of 50 mHz ($L \sim 1.8$, [*Waters et al.*, 1994]) implies an error of ~8% in ρ_o (see equation (4)).

[7] In order to have an idea of the error which may result from an erroneous choice of m, we show in Table 2 for different L-shells the ratio between the eigenvalues when $m = 0$, 6 (which is usually considered the likely range for m) and the eigenvalue for $m = 3$. Since the estimated ρ_o is proportional to λ (equation (4)), the values reported in the second and third columns correspond to the confidence limits of the ratio between the effective ρ_o value and the estimate using $m = 3$. Note that the decrease of the deviation with decreasing L can be misleading because, as we will see better in the following, the heavier ionospheric plasma (mainly O^+) makes a contribution to the field line eigenperiod which increases with decreasing L [*Hattingh and Sutcliffe*, 1987; *Sutcliffe et al.*, 1987; *Poulter et al.*, 1988]. This may cause a larger variability at low latitudes of the effective m value with respect to midlatitudes. Indeed, it has been often pointed out [*Green et al.*, 1993; *Price et al.*, 1999; *Denton and Gallagher*, 2000; *Clilverd et al.*, 2003] that the standard technique for inferring ρ_o may break down for $L < \sim 2$. Investigating in more detail this problem and evaluating the level of accuracy in the ρ_o estimates from low-latitude observations is the main objective of the present paper.

2. Tests of the Remote Sensing Technique Using a Plasmaspheric Density Model

2.1. Model Description

[8] In order to test how reliable the ρ_o inference is when assuming the radial power law (3) we have used a physical-numerical model of the coupled ionosphere-plasmasphere system [*Förster and Jakowski*, 1988; *Jakowski and Förster*, 1995]. This model has been already used for an event study by *Vellante et al.* [2002] who found that the field line eigenfrequencies predicted by the model were in reasonable agreement with those observed at $L = 1.5$–1.9. The model describes the plasma behavior along a given flux tube from 120 km altitude in the northern E region ionosphere through the plasmasphere and down to 120 km altitude in the magnetically conjugate Southern Hemisphere. The flux tube geometry is that of a static geocentric dipole field which is tilted with respect to the Earth's rotation axis. In essence, it is a one-dimensional model solving the following hydrodynamic equations along one particular flux tube. Within ionospheric altitudes (up to 620 km) at both ends of the

Table 2. Range of Variability of the Fundamental Toroidal Eigenvalue

L	$\lambda(m = 0)/\lambda(m = 3)$	$\lambda(m = 6)/\lambda(m = 3)$
1.5	1.10	0.89
2	1.14	0.84
2.5	1.15	0.81
3	1.16	0.80
4	1.17	0.78
5	1.18	0.77
7	1.18	0.75
10	1.19	0.75

flux tube, the continuity and momentum equations of the molecular ions N_2^+, NO^+, and O_2^+ are solved forming the so-called diffusion equations. The model uses the continuity, momentum, and heat conduction equations of the atomic ions H^+, He^+, and O^+, as well as the electron heat conduction equation and simplified kinetic transport equations for the suprathermal electron component along the whole selected flux tube. The model uses the standard empirical neutral gas model MSIS-86 [*Hedin*, 1987] and the empirical neutral wind model HWM93 [*Hedin et al.*, 1996] and can be run for any given seasonal, solar, and geomagnetic conditions. The calculations start at 1200 LT (midday of model day 0) with an initial condition of a nearly empty plasmaspheric flux tube and proceed throughout several days with the same external conditions. The model is similar to the FLIP [*Richards et al.*, 2000] and SUPIM [*Bailey and Balan*, 1996] plasmasphere models, but $\boldsymbol{E} \times \boldsymbol{B}$ drifts are not considered.

[9] For our study we considered seven different L values: 1.61, 1.71, 1.83, 2.39, 2.66, 2.90, 3.31. These particular values have been chosen to correspond to the L values of the field lines midway some station pairs of European BGS, SAMNET (http://samsun.york.ac.uk/), and SEGMA [*Vellante et al.*, 2004] magnetometer arrays. Thus they correspond to magnetic shells which are involved when applying the standard cross-phase technique to measurements from these arrays. For each L value, the dipole field line considered crosses the geomagnetic equator at the same radial distance as the IGRF line starting at 120 km above the considered point. *Hattingh and Sutcliffe* [1987] found that the eigenperiods of such dipole field lines (in the range of L values from 1.3 to 3.0) differed by less than 10% from those computed using the IGRF lines.

[10] We also considered several test cases by varying different conditions (season, LT, solar irradiance, geomagnetic activity, stage of flux tube refilling). However, in this paper we mainly refer to two different cases corresponding to solar minimum (case A) and solar maximum (case B) conditions.

[11] The complete list of the parameters adopted in the two cases is summarized in Table 3. Here $\langle F_{10.7} \rangle$ and $F_{10.7}$ are the 3-month average and the diurnal value of the 10.7 cm solar radio flux. In both cases we considered moderate geomagnetic activity ($K_p = 4$) and almost saturated flux tubes (model day 8). Although we have used equinox conditions, the state of the ionosphere at the two field line footprints is different due to the tilted dipole axis. This causes some hemispheric asymmetry. In order to simplify the discussion we artificially generated symmetric conditions for the two hemispheres by averaging at each altitude the north and south hemispheric density. Therefore in the following we will consider only a single hemisphere. In any case, as we will discuss later in section 2.7, such a procedure does not affect significantly the basic results of our investigation.

2.2. Comparison Between Model Density and Power Law Dependences

[12] In Figure 1 we show for case A a comparison between model field-aligned density profiles (at $L = 2.66$ in Figure 1a, and $L = 1.61$ in Figure 1b) and different power law dependences ($m = 0.5, 1.5, 2.5, 3.5, 4.5, 5.5, 6.5$). The distance along the field line is computed from 120 km altitude up to the equatorial point. As can be seen, the model profile at $L = 2.66$ is well approximated by the radial power law $r^{-0.5}$ in the outer part of the field line (for almost two-thirds of the whole length). As we will see better in the following, the strong discrepancy between the model and the power law dependence in the inner part is not so important for the purpose of sensing the equatorial density. However, the situation at $L = 1.61$ is quite different. No single power law approximates satisfactorily the model profile except for a small region around the equator ($s/s_o > 0.6$) where the model profile is bracketed between the $r^{-2.5}$ and $r^{-3.5}$ curves.

[13] The goodness of a power law approximation can be investigated looking at the variation of the local power law index $m_{loc}(r) = -d \log(\rho)/d \log(r)$. For a radial power law r^{-m}, m_{loc} would be constant and equal to m. Figure 2a shows the behavior of m_{loc} along five field lines for the same conditions considered in Figure 1. As can be seen, for $L > 2$, m_{loc} is almost constant ($0 < m_{loc} < 1$) along the whole second half of the field line. At lower L the slope varies more rapidly, and therefore no single power law can be assigned for any extended part of the field line. In Figure 2b we show the results for case B representative of solar maximum conditions. With respect to the previous case, the slopes are higher and have an appreciable variation in the equatorial region also for $L > 2$.

2.3. A Test Using a Single Eigenfrequency

[14] We now present a test of the standard remote sensing method using simulated eigenfrequencies. For this purpose, for any given model density profile we computed the corresponding toroidal mode eigenfrequencies solving equation (1). These frequencies were simulated to correspond to experimentally measured resonant frequencies. Using (4), an inference of the equatorial mass density assuming different power law dependencies was obtained and compared to the value provided by the model. *Denton and Gallagher* [2000] conducted a similar test by using as model density profiles those provided by the Global Core Plasma Model [*Gallagher et al.*, 2000].

Table 3. Conditions Used for the Two Case Studies

Case	$\langle F_{10.7} \rangle$	$F_{10.7}$	K_p	Season	LT	Model Day
A	85	100	4	March equinox	1200	8
B	185	170	4	March equinox	1200	8

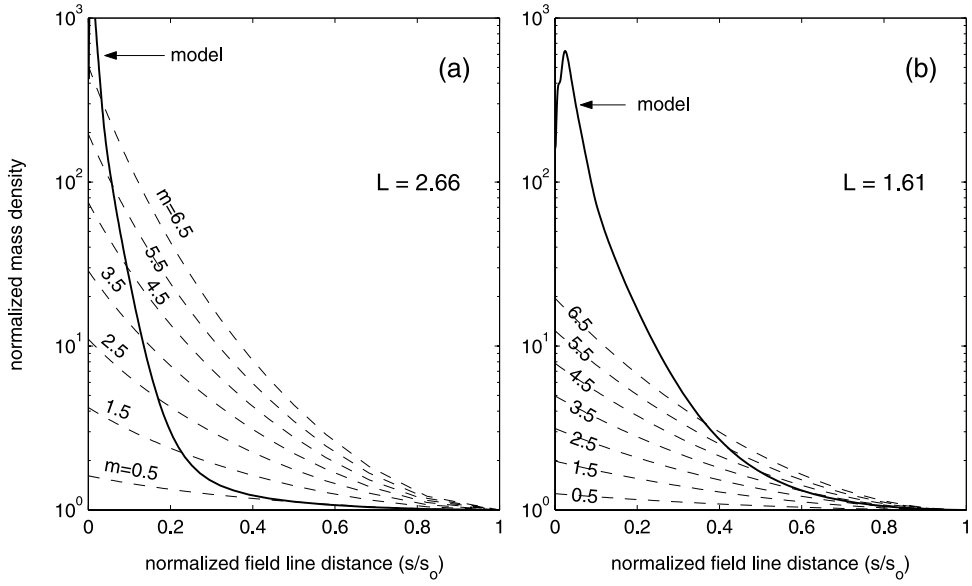

Figure 1. (a) Mass density profile (solid line) along the L = 2.66 field line as derived by the plasmasphere model for case A conditions. Dashed lines correspond to different power law dependences r^{-m} with power index m indicated by the label. (b) The same as Figure 1a but for the L = 1.61 field line.

[15] The results of our test for case A and case B are presented in Figure 3a and Figure 3b, respectively. In each plot the equatorial profile of the mass density as provided by the model (solid line) and that inferred by the remote-sensing technique assuming a given m value (dashed line) are shown. Table 4 provides the percentage deviations δ of the inferred density with respect to the model value. Deviations larger than 15% have been marked; such deviations can be considered comparable (or larger) than typical experimental errors (see section 1). The last column of the table indicates the power law index m_{best} which would provide the right inference. For the solar minimum conditions (case A), a very good agreement is obtained in the range $1.83 < L < 3.31$ using $m = 1$ (deviations within 5%). As m is increased, we obtain better estimates at the lowest L-shells but get significant underestimates at $L > 2$ when $m > \sim 4$. For the solar maximum conditions (case B), $m = 1$ is still a good choice for the four highest L-shells, but it would provide an error of ~30% already at $L = 1.83$ and an error greater than 50% at $L = 1.61$. The commonly used value $m = 3$ would provide good estimates in the central part of the array, but an underestimate of 12% at $L = 3.31$ and an overestimate of 45% at $L = 1.61$.

[16] We then conclude that using a unique power law index for estimating the equatorial density from an extended latitudinal array may lead to incorrect results, i.e., distorted density profiles. The problem concerns mainly the lowest-latitude stations ($L < 2$), which require higher power indices to get a correct estimate. However, at higher latitudes any power index between 0 and 1 would produce reasonable ρ_o estimates. It is also worth noting that for these L-shells the m_{best} values closely correspond to the actual slope of the profiles in the outer part of the field line, i.e., the remarkably different radial dependence of the inner part seems to have no influence. Conversely, at lower L the m_{best} values are significantly higher than $m_{loc}(r_o)$, which means that the density dependence at low altitudes plays an important role.

[17] The results of Table 4 also show that the rate at which the density varies along low-latitude field lines depends significantly on the solar irradiance. For example at $L = 1.61$, m_{best} is 5.9 and 9.8 for case A (solar minimum) and case B (solar maximum), respectively. This means that at these low latitudes, it might be a problem to deduce from the temporal variations of f_R the corresponding correct variations of the equatorial plasma mass density. For example, if we adopted for $L = 1.61$ the fixed value $m = 3$, we would obtain overestimates of ρ_o of 14% and 45% for case A and case B, respectively. As a consequence, a biased dependence of the equatorial density on the solar irradiance would be obtained: $(\rho_{o,B}/\rho_{o,A})_{inferred} = 1.27 \times (\rho_{o,B}/\rho_{o,A})_{actual}$. Note that if one assumes a fixed functional dependence at a given L, it follows from (4) that $(\rho_{o,B}/\rho_{o,A})_{inferred} = (f_{R,A}/f_{R,B})^2$; i.e., the same density ratio is inferred whatever power law index is chosen. Using this simple expression, *Vellante et al.* [1996] deduced a general increase of the plasmasphere density along the local field line ($L \sim 1.6$) by a factor of ~2 from minimum to maximum solar activity. According to present results, the corresponding factor at the equatorial distance might have been ~20–30% lower.

[18] We further examined this aspect by considering the results of the inference for other kinds of temporal variation of the plasmaspheric density which are typically investigated (LT variation and flux tube refilling after a period of intense geomagnetic activity). The results are summarized in Table 5. The second column lists the model result of the ratio of the equatorial density between two different conditions (specified below), the third column lists the corresponding inference as provided by the computed f_R values: $(\rho_{o,2}/\rho_{o,1})_{inferred} = (f_{R,1}/f_{R,2})^2$, and the fourth column

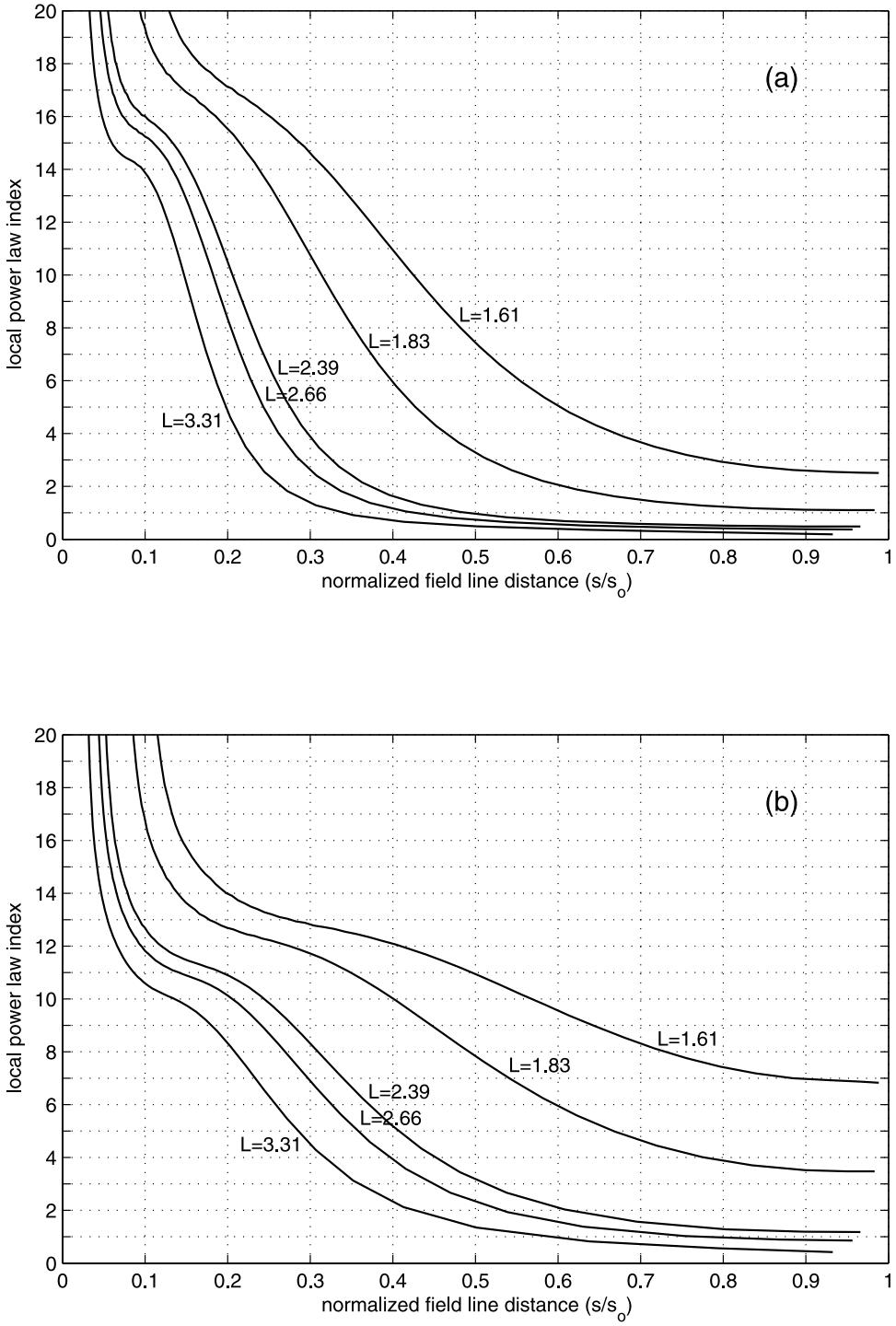

Figure 2. (a) The behavior of the local power law index $m_{\mathrm{loc}}(r) = -d \log(\rho)/d \log(r)$ along different field lines for case A conditions. (b) The same as Figure 2a but for case B conditions.

gives the percentage deviation between the inferred and the actual model density ratio. Only two magnetic shells have been considered. The first case corresponds to a hypothetical comparison between solar minimum and solar maximum conditions which we have already discussed for $L = 1.61$ in the previous paragraph. For $L = 2.66$, the inference correctly gives a negligible solar cycle variation of ρ_o. Slightly higher errors in the inferred solar cycle variation were obtained at all L values when comparing more extreme conditions of solar irradiance. A more detailed investigation on the solar irradiance dependence of field line resonances will be done in a separate paper.

[19] The next two cases correspond to an investigation of the LT variation. We actually considered in all test cases only three different LT values (0600, 1200, 1800). We

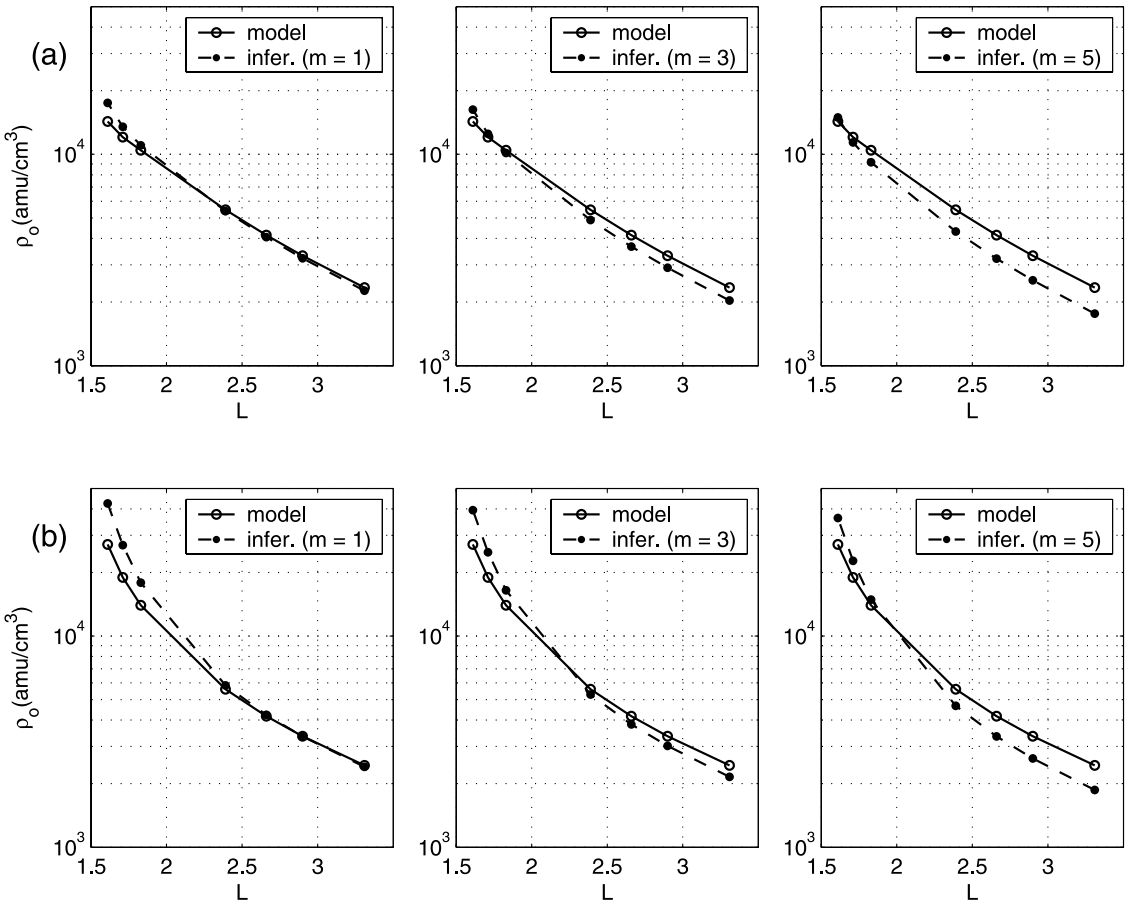

Figure 3. A comparison between model profiles of the equatorial mass density (solid lines) and those inferred by the remote-sensing technique using different power law indices (dashed lines). (a) Case A and (b) case B conditions.

found that for any external condition examined, the rate of falloff of the mass density along the field line (as quantified by the m_{best} index) was minimum, maximum, and intermediate for 0600 LT, 1200 LT, and 1800 LT, respectively. The comparison between 0600 and 1200 LT for both solar minimum and solar maximum conditions is presented in Table 5. As can be seen, the diurnal density increase would be a little bit overestimated at the inner L-shell. Note that for both the solar cycle and diurnal variation, the mass density change at the equator is overestimated because the change of ρ is not uniform along the field line. As a matter of fact, the model predicts a maximum relative change of ρ (somewhat higher than at the equator) at a quite lower altitude ($\sim$2000 km).

[20] The last two cases of Table 5 correspond to a simulated comparison of conditions during two different phases of plasma refilling after a period of intense geomagnetic activity. This is done by comparing the results for model days 3 and 8. For L = 1.61, an almost saturated flux tube condition is reached already on the third day, so there are not appreciable differences on model day 8. For L = 2.66, the significant density increase (of a factor $\sim$2) occurring between day 3 and day 8 is correctly estimated both for solar minimum and solar maximum conditions.

2.4. Integral Form of the Field Line Eigenperiod

[21] The results of the previous section show that the low-altitude plasma has a small influence on the midlatitude field line eigenperiods. This is generally explained in the

Table 4. Percentage Difference Between Inferred and Actual Equatorial Density As Obtained By the Model for Different L-Shells and Power Law Density Indices[a]

	m = 0	m = 1	m = 2	m = 3	m = 4	m = 5	m = 6	
L	δ, %	δ, %	δ, %	δ, %	δ, %	δ, %	δ, %	m_{best}
				Case A				
3.31	+1	−3	−8	−13	**−19**	**−25**	**−31**	0.3
2.90	+2	−3	−7	−12	**−18**	**−24**	**−30**	0.4
2.66	+2	−2	−7	−12	**−17**	**−23**	**−29**	0.5
2.39	+3	−1	−6	−11	**−16**	**−21**	**−27**	0.7
1.83	+9	+5	+1	−3	−7	−12	**−17**	2.3
1.71	**+16**	+12	+8	+4	−0.9	−6	−11	3.8
1.61	**+27**	**+22**	**+18**	+14	+9	+5	−0.4	5.9
				Case B				
3.31	+3	−2	−6	−12	**−17**	**−23**	**−30**	0.7
2.90	+4	−0.1	−5	−10	−15	**−21**	**−28**	1.0
2.66	+6	+1	−3	−8	−14	**−20**	**−26**	1.3
2.39	+9	+4	−0.5	−6	−11	**−17**	**−23**	1.9
1.83	**+33**	**+28**	**+23**	**+18**	+12	+6	+0.4	6.1
1.71	**+47**	**+42**	**+37**	**+31**	**+26**	**+20**	+13	8.0
1.61	**+61**	**+56**	**+51**	**+45**	**+39**	**+33**	**+27**	9.8

[a]Deviations larger than 15% are marked in bold.

Table 5. A Comparison of Model and Inferred Temporal Variations of the Equatorial Plasma Mass Density

L	$(\rho_{o,2}/\rho_{o,1})_{model}$	$(\rho_{o,2}/\rho_{o,1})_{inferred}$	δ, %
	1: SOL MIN, 2: SOL MAX (1200 LT, Eighth Day)		
2.66	1.01	1.04	+4
1.61	1.90	2.42	+27
	1: 0600 LT, 2: 1200 LT (SOL MIN, Eighth Day)		
2.66	1.07	1.07	+0.4
1.61	1.35	1.49	+11
	1: 0600 LT, 2: 1200 LT (SOL MAX, Eighth Day)		
2.66	1.15	1.18	+3
1.61	1.86	2.16	+16
	1: Third Day, 2: Eighth Day (SOL MIN, 1200 LT)		
2.66	1.94	1.93	−0.8
1.61	1.07	1.05	−2
	1: Third Day, 2: Eighth Day (SOL MAX, 1200 LT)		
2.66	1.74	1.64	−5
1.61	1.03	1.01	−3

framework of the time of flight or WKB approximation [*Warner and Orr*, 1979]. In this approach the period of the fundamental standing wave is considered to correspond to the time taken by an Alfvén wave to travel along the field line between the opposite ionospheres and back:

$$T_{WKB} = 2\int_{P_1}^{P_2} \frac{ds}{V_A(s)} \tag{5}$$

where V_A is the Alfvén velocity, and the integration is performed along the field line between the two conjugate points P_1 and P_2 where the wave is reflected (at the ionospheric altitude). In the terms of the z coordinate:

$$T_{WKB} = \frac{L^4}{\pi C}\int_{-z_i}^{z_i} \left(1-z^2\right)^3 \rho(z)^{1/2} dz \tag{6}$$

For midlatitude field lines, the Alfvén velocity is minimum in the equatorial region, so it follows from (5) that the density in such region will provide the major contribution to the eigenperiod [*Poulter et al.*, 1988].

[22] In order to clarify this argument, we show in Figure 4 the model profiles of $1/V_A$ (solid line) along the two field lines $L = 2.66$ (left) and $L = 1.61$ (right). External conditions are those of case A. We also show the $1/V_A$ profiles corresponding to density distributions $\propto r^{-m_{best}}$ (dashed line) and $r^{-m_{WKB}}$ (dotted line) where m_{WKB} is the exponent providing the same time of flight (i.e., the areas under the solid and dotted lines are the same). As can be seen, along the $L = 2.66$ field line the profile corresponding to $m = m_{best} = 0.5$ follows the model profile very well in the outer part of the field line (see also Figures 1a–2a). However, in the model profile the contribution of the inner part ($s/s_o < 0.2$) to T_{WKB} is not negligible and a higher exponent ($m = m_{WKB} = 2.6$) is necessary to obtain the same time of flight. This effect is obviously even more evident at $L = 1.61$ where the ionospheric contribution is stronger.

[23] The discrepancy between m_{best} and m_{WKB} simply comes from the reason that in general the time-of-flight approximation is not an accurate estimate of the toroidal eigenperiod (except for the special case $\rho \propto r^{-6}$ when the two values coincide [*Radoski*, 1966]). For example, for the model profiles shown in Figure 4, T_{WKB} differs from the actual eigenperiod (as computed by equation (1)) of −17% and +42% for $L = 2.66$ and $L = 1.61$, respectively.

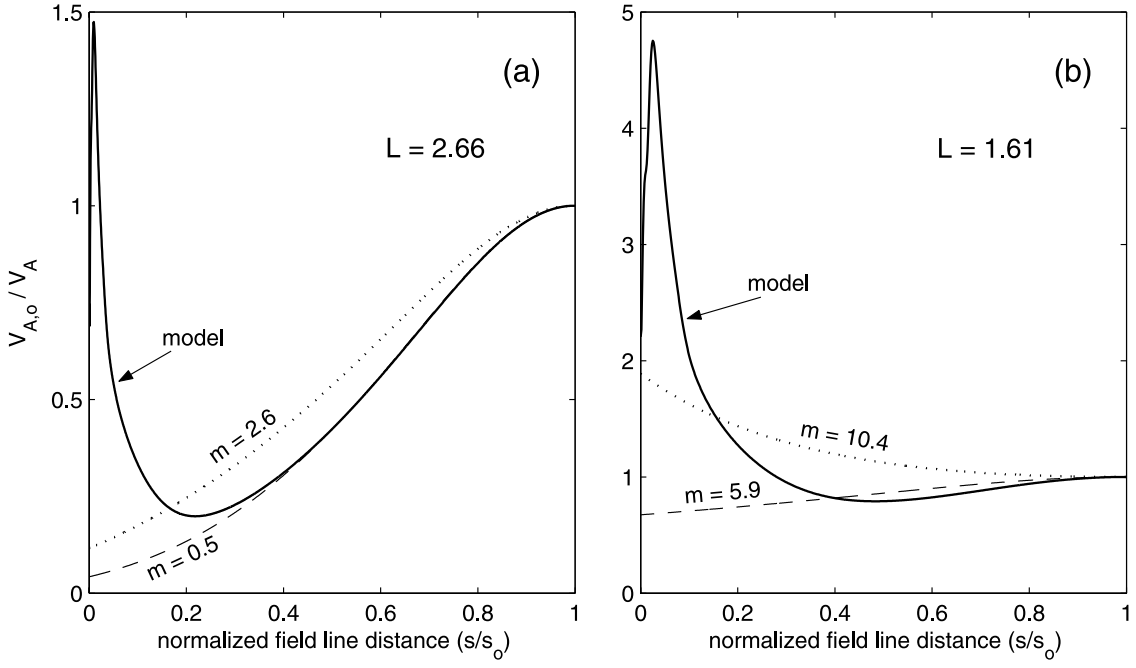

Figure 4. (a) Profiles of V_A^{-1} along the $L = 2.66$ field line for the case A model (solid line), and density distributions $\propto r^{-m_{best}}$ (dashed line) and $r^{-m_{WKB}}$ (dotted line). See the text for the definition of the indices m_{best} and m_{WKB}. (b) The same as Figure 4a but for the $L = 1.61$ field line.

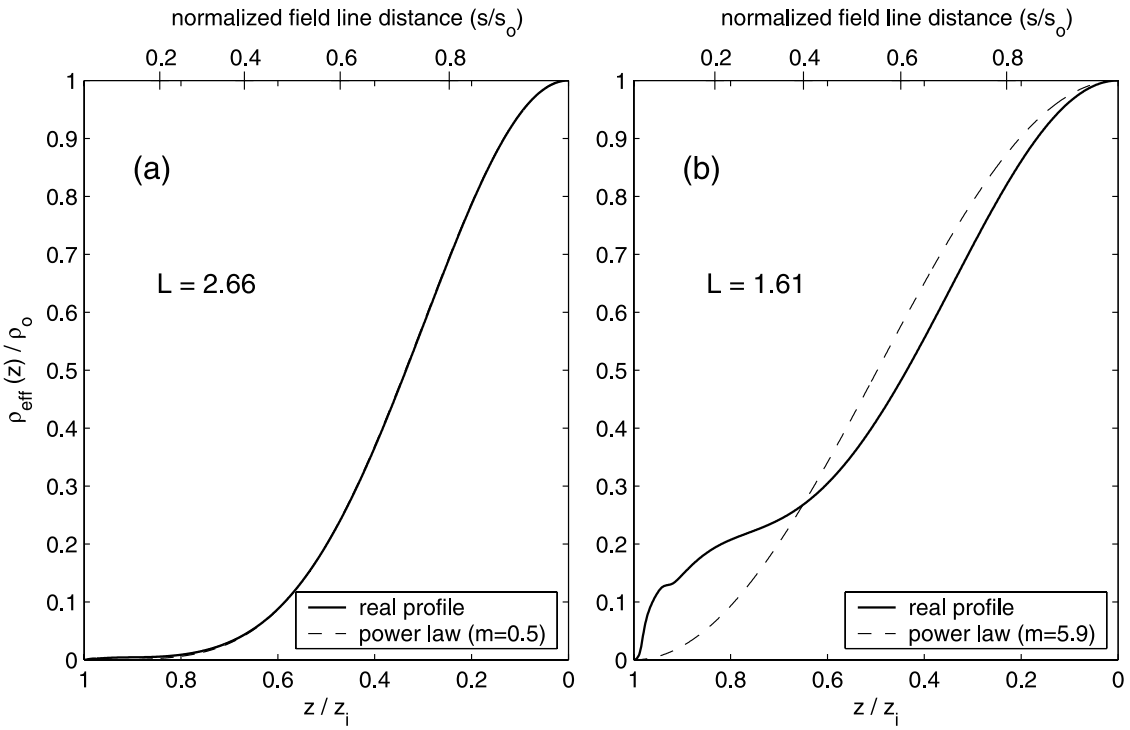

Figure 5. (a) Profiles of the effective plasma mass density (integrand of equation (8)) along the $L = 2.66$ field line for the case A model (solid line), and a density distribution $\propto r^{-m_{best}}$ (dashed line). (b) The same as Figure 5a but for the $L = 1.61$ field line.

[24] In order to get a more correct evaluation of the different contributions along the field line we have followed the approach of *Taylor and Walker* [1984]. They found accurate estimates of the toroidal eigenvalues for density distributions varying as r^{-m} by applying a perturbation method. We have generalized their procedure for any given density distribution. Similarly to *Taylor and Walker* [1984], we write equation (1) in the form:

$$\frac{d^2\varepsilon(z)}{dz^2} + [1 - \eta(z)]\lambda\varepsilon(z) = 0 \qquad (7)$$

where the perturbation term $\eta(z) = 1 - (1 - z^2)^6\ [\rho(z)/\rho_o]$.

[25] Using equations (4) and (5) of *Taylor and Walker* [1984], we find straightforwardly the following first-order approximation of the fundamental toroidal eigenperiod:

$$T \cong \frac{L^4}{\pi C}\left[4z_i \int_{-z_i}^{z_i} \left(1 - z^2\right)^6 \cos^2\left(\frac{\pi}{2}\frac{z}{z_i}\right)\rho(z)dz\right]^{1/2} \qquad (8)$$

We have verified that this expression gives an excellent approximation of the actual toroidal eigenperiod. For example, for the model profiles shown in Figure 4, the expression (8) overestimates the actual eigenperiod of only 0.9% and 0.5% for $L = 2.66$ and $L = 1.61$, respectively. With respect to the WKB approximation (6), the expression (8) contains the factor $\cos^2\left(\frac{\pi}{2}\frac{z}{z_i}\right)$ which is zero at the line footprints ($z = \pm z_i$), so the high-density values at ionospheric levels are strongly attenuated by this factor.

[26] To better illustrate this behavior, we plot in Figure 5 the effective distribution of the plasma density $\rho_{eff}(z) = (1 - z^2)^6 \cos^2\left(\frac{\pi}{2}\frac{z}{z_i}\right)\rho(z)$ (the integrand of (8)) normalized at $z = 0$, again for the conditions of case A. We also show the corresponding profile for a density distribution $\propto r^{-m_{best}}$ (dashed line). As can be seen (compare with Figure 1 and Figure 4), at $L = 2.66$ the power law $r^{-0.5}$ is indistinguishable from the real profile and a very small contribution ($\sim$1%) to the eigenperiod (the square root of the area under the curves) is given by the plasma within the region $z/z_i > 0.6$ (i.e., for altitudes $< \sim$7000 km, or latitudes $> \sim$30°). At $L = 1.61$, the power law $r^{-m_{best}}$ does not fit the real profile as well as for the higher L-value. Therefore at these low latitudes, the index m_{best} has to be considered only as an effective index producing the right estimate of the equatorial density from the observed eigenfrequency, but it does not represent the real density variation in any extended part of the field line (see also Figure 2). In this case the ionospheric contribution is more significant. For example, the total plasma tube below an altitude of $\sim$2000 km (corresponding to $z/z_i > 0.7$, or latitude > $\sim$25°) gives a contribution to the eigenperiod of about 5% ($\sim$6% for case B).

2.5. A Test Using Both the Fundamental and the Second Harmonic

[27] The knowledge of other harmonics, in addition to the fundamental, can provide important information about the density distribution along the field line and then a more reliable estimate of ρ_o. This method has been applied using observed toroidal harmonics in satellite measurements [*Takahashi and McPherron*, 1982; *Denton et al.*, 2001; *Takahashi et al.*, 2004] and from midlatitude ground-based observations [*Fedorov et al.*, 1990]. At low latitudes ($L < 2$) evidence of higher harmonics is rarely found in ground

Table 6. Results of the Test Using Both the First and the Second Harmonic[a]

L	f_2/f_1	m_{inferred}	δ, %	δ, % – Schulz
		Case A		
3.31	2.52	0.3	−0.2	+0.5
2.90	2.49	0.5	−0.3	−0.1
2.66	2.46	0.6	−0.4	−0.6
2.39	2.42	0.8	−0.7	−1
1.83	2.15	3.9	−7	−9
1.71	1.96	6.6	−14	−13
1.61	1.77	9.5	**−20**	−14
		Case B		
3.31	2.49	0.8	−0.8	−0.6
2.90	2.43	1.2	−1	−2
2.66	2.38	1.7	−2	−3
2.39	2.29	2.6	−4	−5
1.83	1.82	8.2	−14	−11
1.71	1.70	10.0	−15	−6
1.61	1.62	11.5	−14	+0.1

[a]Deviations larger than 15% are marked in bold.

observations [*Green et al.*, 1993; *Waters et al.*, 1994; *Pilipenko et al.*, 1998; *Menk et al.*, 2000; *Vellante et al.*, 2002], so we limited testing of the remote-sensing technique to cases when both the fundamental and second harmonic are realistically available. For a power law dependence (3), and for any L value, there is a unique correspondence between the frequency ratio f_2/f_1 of the second harmonic over the fundamental frequency and the exponent m.

[28] The results of our test for the usual cases A and B are shown in Table 6. The second column shows the frequency ratio f_2/f_1 as obtained by solving the toroidal wave equation (1) for the given plasma density distribution. The third column lists the power index m_{inferred} corresponding to that frequency ratio. The fourth column gives the percentage error of the ρ_o estimate assuming a power law density distribution with the inferred m value of column 3. The last column gives the percentage error of the ρ_o estimate obtained using equation (8) of *Schulz* [1996]. Using our notation, the *Schulz* formula is

$$\tilde{\rho}_o = \left(\frac{3\pi C}{8 z_i L^4 f_{3/4}}\right)^2 \tag{9}$$

where $f_{3/4}$ is the extrapolation to $n = 3/4$ of a linear fit of the eigenfrequencies f_n versus the harmonic number n. In our case, having considered only the first two harmonics, $f_{3/4} = (5f_1 - f_2)/4$.

[29] For case A, as expected from the previous analysis, the good approximation of the real density profile with a power law distribution (for $L > 2$) makes the inferred power law index very close to the actual index characteristic of the outer part of the field line. As a consequence, the value of ρ_o inferred from both methods is in excellent agreement (difference within 1%) with the actual model value. Conversely, for $L < 2$ the index is somewhat overestimated, and the error in the ρ_o estimate provided by the first method reaches 20% at $L = 1.61$. Unexpectedly, for this L shell, the estimate provided by the Schulz's formula is somewhat better ($\delta = -14\%$). This is not totally surprising because the estimate provided by the first method should be better than the Schulz estimate only if the density distribution is closely fitted by a power law.

[30] For case B, the accuracy of the ρ_o estimates for $L > 2$ is only slightly lower with respect to case A ($\delta < 5\%$). Conversely, a better estimate is obtained at the lowest latitude ($L = 1.61$). Again, we find a better estimate when using the Schulz's expression not only at $L = 1.61$ (where the discrepancy is only 0.1%) but also at $L = 1.71$ and $L = 1.83$. So, for our low-latitude model density distributions, the Schulz approximation seems partially to counterbalance the error which comes from assuming that these distributions follow a power law. We considered other conditions different from those of cases A and B, and we verified that the previous circumstance is always true at $L = 1.61$. In particular we find that the Schulz's estimate provides a more significant improvement for steeper variations of the field-aligned density.

[31] It must be remarked however that, when analyzing real data, the use of higher harmonic frequencies increases the random error associated with ρ_o. For example, using the fundamental and second harmonic, and assuming independent estimates of f_1 and f_2 with the same relative error $\delta f/f$, we obtain from (9):

$$\frac{\delta\rho_o}{\rho_o} = \frac{2\left[1 + (f_2/5f_1)^2\right]^{1/2}}{1 - (f_2/5f_1)} \frac{\delta f}{f} \tag{10}$$

If we set $f_2/f_1 = 2.5$ (a proper value for $L \sim 3$, see Table 6) we get $\delta\rho_o/\rho_o \sim 4.5\ \delta f/f$, while setting $f_2/f_1 = 1.7$ ($L \sim 1.6$) we get $\delta\rho_o/\rho_o \sim 3\ \delta f/f$. Note that when only one frequency is used, $\delta\rho_o/\rho_o = 2\ \delta f/f$. Similar random error estimates were obtained by *Denton and Gallagher* [2000] using a Monte Carlo simulation.

2.6. Test of the *Price et al.* [1999] Technique

[32] A different approach to infer the plasma mass density from low-latitude field line resonances was proposed by *Price et al.* [1999]. Their method uses a finite difference approximation of the toroidal wave equation to infer the mass density at discrete locations along a magnetic field line without assuming any functional dependence for the plasma distribution. We conducted a test of this technique using our density models. As suggested by the authors, we used the first three harmonics. Assuming symmetry between the Northern and Southern Hemispheres (a condition which is satisfied by our density distributions) the mass density is evaluated at three different points of the field line, i.e., at geomagnetic latitudes: 1/7 Λ, 3/7 Λ, and 5/7 Λ, where Λ is the latitude where a perfect reflection of the wave is assumed to occur ($\sin\Lambda = z_i$). The resulting estimates are then compared with the actual model values.

[33] The results of this comparison are shown in Table 7. The values in the second, fourth, and sixth columns are the altitudes where the density is estimated, while the values in the third, fifth, and seventh columns are the corresponding percentage differences of the density estimates with respect to the actual model values. Results are not reported for $L = 3.31$, 2.90, 2.66, and $L = 2.39$ (case A) because the iterative process required for solution failed to converge. Failures to reach the convergence in the iterative process involved in this technique are also reported by *Price et al.* [1999] for

Table 7. Results of the Test Using the *Price et al.* [1999] Technique[a]

L	h_1, km	δ_1, %	h_2, km	δ_2, %	h_3, km	δ_3, %
			Case A			
1.83	2406	**+43**	4188	**−18**	5162	**−26**
1.71	2091	**+49**	3601	**−37**	4418	**−19**
1.61	1824	**+49**	3108	**−62**	3798	−9
			Case B			
2.39	3804	−2	6882	−2	8628	**−37**
1.83	2406	**+21**	4188	**−36**	5162	**−23**
1.71	2091	**+21**	3601	**−46**	4418	−15
1.61	1824	**+21**	3108	**−51**	3798	−9

[a]Deviations larger than 15% are marked in bold.

some combinations of the harmonic ratios f_2/f_1 and f_3/f_2. In our analysis the technique did not work for the highest L values which are characterized by higher harmonic ratios (i.e., flatter density profiles). We have not investigated further this aspect since we were mainly interested in the results for the lowest L values where the density inference obtained by the standard techniques discussed in the previous sections is more problematic. The density estimates obtained at the highest altitude (h_3, corresponding to a geomagnetic latitude less than 7°) can be practically considered to be an estimate of the equatorial density ρ_o, since at these latitudes the mass density is expected to be only slightly higher than ρ_o. As can be seen, the estimates obtained at h_3 improve with decreasing L and become satisfactory (9% discrepancy for both cases) at L = 1.61. An opposite trend is observed at the other altitudes where the estimates, with the exception of case B at L = 2.39, are generally poor. Similar results were obtained for other test cases; in particular we found that the error in the estimate of $\rho(h_3)$ at L = 1.61 was always within ∼15%. A general underestimate of $\rho(h_3)$ was also confirmed.

2.7. Hemispheric Asymmetry and E × B Drift Effects

[34] As discussed in section 2.1, we have considered, throughout the paper, hemispheric symmetry conditions by artificially averaging, at each altitude, the density of the two hemispheres. By doing so, we have not changed significantly the basic shape of the field-aligned density profiles which is the essential element for testing the validity of the remote-sensing techniques which assume a power law falloff of the mass density along the field lines.

[35] Nevertheless, in order to check how hemispheric asymmetries may affect our results, we have also analyzed the original density profiles generated by the model. Figure 6 illustrates the hemispheric density asymmetry along the L = 1.61 field line for case A. In this case the mass density is higher in the Southern Hemisphere with a maximum discrepancy at an altitude of ∼1500 km ($s/s_o \cong 0.25$) where $\rho_{South}/\rho_{North} \cong 1.7$. This kind of asymmetry is similar to that one examined by *Poulter et al.* [1990], although their procedure was opposite to ours. They started, indeed, from an original symmetric (equinoctial) aligned dipole field which was then artificially modified by reducing the density by a constant factor in one hemisphere, with a smooth matching at the equator. They found that the introduced asymmetry distorted the standing waveform and shifted the node/antinode positions, but no quantitative indication about eigenfrequency changes was given. For the case illustrated in Figure 6, we find that the first three eigenfrequencies differ from the corresponding eigenfrequencies of the artificial symmetric profile by only 0.4%, 2%, and 2%. These differences decrease with increasing L and become completely negligible at $L > 2$ where the different conditions of the opposite ionospheres do not produce any appreciable hemispheric asymmetry in the outer part of the field line. Similar differences are found also for Case B. Slightly larger effects are found for a more pronounced asymmetry corresponding to northern winter conditions. In that case the maximum asymmetry is found, for L = 1.61, at an altitude of ∼1800 km ($s/s_o \cong 0.3$) where the Southern Hemisphere mass density is higher than the Northern Hemisphere one by a factor of ∼3. In this case, the first three eigenfrequencies change with respect to the artificial symmetric condition by 3%, 3%, and 4%. Therefore even for this more extreme case, the basic conclusions of our investigation would not be appreciably modified.

[36] Another effect which we have not considered in our model is the **E** × **B** drift. *Bailey* [1983] showed that it could affect significantly the daytime plasma concentration at L = 1.4 (about 20% of increase in the O^+ plasma tube content at 12 LT). Also, *Poulter et al.* [1988] showed that the inclusion of **E** × **B** drifts has a significant effect on the field line eigenfrequencies at low and middle latitudes. In addition, *Clilverd et al.* [2000] showed that **E** × **B** drift may produce significant plasmaspheric depletions during geomagnetic storms. However, it is worth to remark that what is important for the purpose of the density inference is the assumed shape of the density profile. If a process has the only effect to uniformly modify the density along the field line by a constant factor, i.e., leaving unaltered the shape of the profile, the relative accuracy in the density estimate would not change, regardless of how big the density change is (equations (1), (2), and (4)). In this regard, *Bailey* [1983, Figure 7] shows that at L = 1.4 the shape of the field-aligned ion density profiles does not change significantly for the effect of the **E** × **B** drift (there appears to be only a slightly higher rate of variation). Analogously, Figure 8 in the paper by *Poulter et al.* [1988], which refers to an L = 4 field line, shows that the **E** × **B** drift, although significant, appears to modify all eigenfrequencies by the same factor (an increase of ∼15% at 1200 LT). The fact that the different harmonic ratios do not appreciably change is indicative of a negligible change of the shape of the density profile too. Also, *Tu et al.* [2003] ran the FLIP model with various constant drift speeds at the equator and found that none of the simulated density profiles exhibited a significant change in off-equatorial density gradients. So we are confident that the inclusion of an **E** × **B** drift effect would only modify the details of the values reported in the different tables but would leave unaltered the observed trends.

3. Conclusions

[37] The knowledge of spatial and temporal variations of the magnetospheric plasma mass density represents essential information for understanding the complex dynamic processes occurring in the magnetosphere. This may be

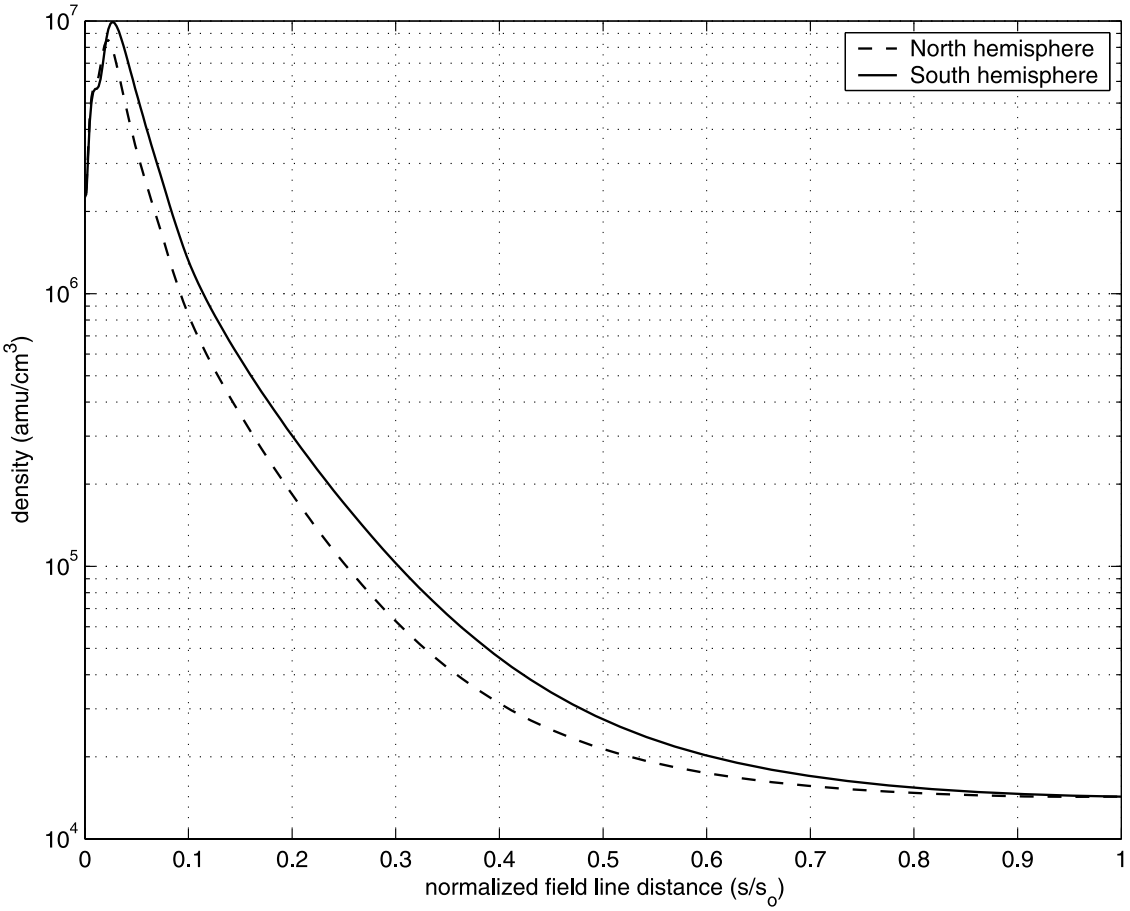

Figure 6. Model mass density profiles (Case A) along the L = 1.61 field line in the Northern and Southern Hemisphere.

accomplished by the remote-sensing technique based on ground ULF wave measurements. Indeed, new extended ground-based magnetometer arrays (SAMBA, http://samba.atmos.ucla.edu; MEASURE, http://measure.igpp.ucla.edu; McMAC, http://spc.igpp.ucla.edu/McMAC/) have this goal as one of the primary objectives. Besides, plasma mass density estimates, when combined with electron density estimates as provided by VLF whistlers or satellite measurements, can provide important constraints on the relative abundances of different ions.

[38] It is then very important to explore the potentialities and limitations of this method and to determine possible biases before using it indiscriminately. We found it useful to conduct such an investigation using a plasmasphere model as a test. The advantage of using such a simulation is that the model provides a complete realistic field-aligned mass density distribution allowing precise evaluation of the corresponding field line eigenfrequencies. From these frequencies it is then possible to make a direct comparison between inferred and actual model densities. The model can also be run for different solar and geomagnetic conditions, allowing us to investigate how the different conditions affect the density estimates obtained by the remote sensing method.

[39] In this paper we have limited our attention to the evaluation of the accuracy in the inferred equatorial mass density when the standard assumption of a radial power law distribution of the field-aligned mass density is used. We found that for midlatitude field lines ($2.4 < L < 3.3$) a power law index of $\sim$1 might be appropriate for a large variety of solar and geomagnetic conditions. This agrees with satellite measurements at somewhat greater L-shells [*Denton et al.*, 2002; *Takahashi et al.*, 2004] and is consistent with a diffusive equilibrium profile [*Angerami and Carpenter*, 1966; *Takahashi et al.*, 2004]. Using an integral form of the field line eigenperiod, we have quantitatively confirmed that for these latitudes the mass loading due to ionospheric O^+ or other ions, like, e.g., He^+, has a negligible influence on the eigenperiod.

[40] At lower latitudes ($L < 2$) the situation is quite different. First of all, since a significant fraction of the field line is in the ionosphere where the radial variation of the plasma density is much steeper, the density profile cannot be approximated satisfactorily by any power law dependence. This is due to a large part of the flux tube being populated by at least two ion species (H^+ and O^+) which have different scale heights. Obviously, for any real profile we can define a fictitious power law index m_{best} which provides the right inference of the equatorial density. At these low latitudes, m_{best} represents a sort of average index which does not correspond to any particular variation along the field line. Even so, it is not possible to determine a unique empirical $m_{best}(L)$ dependence. Ion composition at the ionospheric level is strongly dependent on solar and

geomagnetic conditions and this dependence influences the plasma distribution along the whole field line. We have given some indication how $m_{best}(L)$ might depend on solar irradiance or local time, but our results should be considered with caution and verified by using more sophisticated plasmasphere models [*Bailey and Balan*, 1996; *Richards et al.*, 2000] or even global self-consistent thermosphere-ionosphere-plasmasphere models including electrodynamics (as, e.g., *Namgaladze et al.* [2000]).

[41] The general rapid increase of m_{best} with decreasing L for $L < 2$ may lead to obtaining distorted profiles of the derived equatorial density when the same power law dependence is used for middle- and low-latitude field lines. In this regard, the empirical plasmaspheric mass density model derived by *Berube et al.* [2005] between $L = 1.7$ and $L = 3.2$ likely overestimates the density values at the lowest L values. Such an effect could be also the cause of the unrealistically high rate of decrease of the inferred equatorial mass density between two close L-shells (1.6 and 1.74) recently found by *Zesta et al.* [2004].

[42] For a similar reason, when the same assumption is used to investigate the temporal variation of the equatorial density at a fixed low-latitude field line, one should be aware that the inferred variation might be somewhat overestimated.

[43] The alternative technique proposed by *Price et al.* [1999] is attractive because it does not assume any a priori functional dependence of the plasma distribution. We verified that for the inner shell investigated ($L = 1.61$) this technique provides reasonable estimates of the mass density near the equator. However, this technique has a very limited application since the simultaneous detection of the first three harmonics of the field line resonance is rarely accomplished at low latitudes.

[44] A possible improvement in the inference of the plasmaspheric mass density from low-latitude field line resonances might come from combining ULF wave observations with simultaneous ground-based ionospheric measurements (from ionosondes, incoherent radar, GPS ground stations for TEC determination), as well as by using the best updated plasmasphere models for numerical modeling/simulation. In particular, it would be extremely important, especially for space weather applications, to extend the present investigation (which is based on a climatological model) to the highly dynamic conditions which occur during geomagnetic storms. It would require the inclusion of the $\mathbf{E} \times \mathbf{B}$ dynamics and other storm specific phenomena as, e.g., heating processes, changes in the global neutral wind circulation and in the neutral gas composition which are not adequately reproduced by the MSIS model [see, e.g., *Förster et al.*, 1999; *Clilverd et al.*, 2000; *Namgaladze et al.*, 2000; *Richards et al.*, 2000; *Tu et al.*, 2003].

[45] **Acknowledgments.** Amitava Bhattacharjee thanks Frederick Menk and David Berube for their assistance in evaluating this paper.

References

Allan, W., and F. B. Knox (1979), The effect of finite ionospheric conductivities on axisymmetric toroidal Alfvén wave resonances, *Planet. Space Sci.*, *27*, 939–950.

Angerami, J. J., and D. L. Carpenter (1966), Whistler studies of the plasmapause in the magnetosphere: 2. Electron density and total tube content near the knee in magnetospheric ionization, *J. Geophys. Res.*, *71*, 711–725.

Bailey, G. J. (1983), The effect of a meridional ExB drift on the thermal plasma at $L = 1.4$, *Planet. Space Sci.*, *31*, 389–409.

Bailey, G. J., and N. Balan (1996), A low-latitude ionosphere-plasmasphere model, in *Solar Terrestrial Energy Program (STEP) Handbook of Ionospheric Models*, edited by R. W. Schunk, pp. 173–206, Utah State Univ., Logan, Utah.

Baransky, L. N., J. E. Borovkov, M. B. Gokhberg, S. M. Krylov, and V. A. Troitskaya (1985), High resolution method of direct measurement of the magnetic field lines' eigen frequencies, *Planet. Space Sci.*, *33*, 1369–1374.

Berube, D., M. B. Moldwin, and J. M. Weygand (2003), An automated method for the detection of field line resonance frequencies using ground magnetometer techniques, *J. Geophys. Res.*, *108*(A9), 1348, doi:10.1029/2002JA009737.

Berube, D., M. B. Moldwin, S. F. Fung, and J. L. Green (2005), A plasmaspheric mass density model and constraints on its heavy ion concentration, *J. Geophys. Res.*, *110*, A04212, doi:10.1029/2004JA010684.

Carpenter, D. L., and R. L. Smith (1964), Whistler measurements of electron density in the magnetosphere, *Rev. Geophys.*, *2*, 415–441.

Chi, P. J., C. T. Russell, S. Musman, W. K. Peterson, G. Le, V. Angelopoulos, G. D. Reeves, M. B. Moldwin, and F. K. Chun (2000), Plasmaspheric depletion and refilling associated with the September 25, 1998 magnetic storm observed by ground magnetometers at $L = 2$, *Geophys. Res. Lett.*, *27*, 633–636.

Chi, P. J., C. T. Russell, J. C. Foster, M. B. Moldwin, M. J. Engebretson, and I. R. Mann (2005), Density enhancement in plasmasphere-ionosphere plasma during the 2003 Halloween Superstorm: Observations along the 330th magnetic meridian in North America, *Geophys. Res. Lett.*, *32*, L03S07, doi:10.1029/2004GL021722.

Clilverd, M. A., B. Jenkins, and N. R. Thomson (2000), Plasmaspheric storm time erosion, *J. Geophys. Res.*, *105*, 12,997–13,008.

Clilverd, M. A., et al. (2003), In situ and ground-based intercalibration measurements of plasma density at $L = 2.5$, *J. Geophys. Res.*, *108*(A10), 1365, doi:10.1029/2003JA009866.

Dent, Z. C., I. R. Mann, F. W. Menk, J. Goldstein, C. R. Wilford, M. A. Clilverd, and L. G. Ozeke (2003), A coordinated ground-based and IMAGE satellite study of quiet-time plasmaspheric density profiles, *Geophys. Res. Lett.*, *30*(12), 1600, doi:10.1029/2003GL016946.

Denton, R. E., and D. L. Gallagher (2000), Determining the mass density along magnetic field lines from toroidal eigenfrequencies, *J. Geophys. Res.*, *105*, 27,717–27,725.

Denton, R. E., M. R. Lessard, R. Anderson, E. G. Miftakhova, and J. W. Hughes (2001), Determining the mass density along magnetic field lines from toroidal eigenfrequencies: Polynomial expansion applied to CRRES data, *J. Geophys. Res.*, *106*, 29,915–29,924.

Denton, R. E., J. Goldstein, J. D. Menietti, and S. L. Young (2002), Magnetospheric electron density model inferred from Polar plasma wave data, *J. Geophys. Res.*, *107*(A11), 1386, doi:10.1029/2001JA009136.

Fedorov, E. N., B. N. Belenkaya, M. B. Gokhberg, S. P. Belokris, L. N. Baransky, and C. A. Green (1990), Magnetospheric plasma density diagnosis from gradient measurements of geomagnetic pulsations, *Planet. Space Sci.*, *38*, 269–272.

Förster, M., and N. Jakowski (1988), The nighttime winter anomaly (NWA) effect in the American sector as a consequence of interhemispheric ionospheric coupling, *Pure Appl. Geophys.*, *127*, 447–471.

Förster, M., A. A. Namgaladze, and R. Y. Yurik (1999), Thermospheric composition changes deduced from geomagnetic storm modeling, *Geophys. Res. Lett.*, *26*, 2625–2628.

Gallagher, D. L., P. D. Craven, and R. H. Comfort (2000), Global core plasma model, *J. Geophys. Res.*, *105*, 18,819–18,833.

Goldstein, J., R. E. Denton, M. K. Hudson, E. G. Miftakhova, S. L. Young, J. D. Menietti, and D. L. Gallagher (2001), Latitudinal density dependence of magnetic field lines inferred from Polar plasma wave data, *J. Geophys. Res.*, *106*, 6195–6201.

Green, A. W., E. W. Worthington, L. N. Baransky, E. N. Fedorov, N. A. Kurneva, V. A. Pilipenko, D. N. Shvetzov, A. A. Bektemirov, and G. V. Philipov (1993), Alfven field line resonances at low latitudes ($L = 1.5$), *J. Geophys. Res.*, *98*, 15,693–15,699.

Hattingh, S. K. F., and P. R. Sutcliffe (1987), Pc 3 pulsation eigenperiod determination at low latitudes, *J. Geophys. Res.*, *92*, 12,433–12,436.

Hedin, A. E. (1987), MSIS-86 thermospheric model, *J. Geophys. Res.*, *92*, 4649–4662.

Hedin, A. E., et al. (1996), Empirical wind model for the upper, middle and lower atmosphere, *J. Atmos. Terr. Phys.*, *58*, 1421–1447.

Huang, X., B. W. Reinisch, P. Song, J. L. Green, and D. L. Gallagher (2004), Developing an empirical density model of the plasmasphere using IMAGE/RPI observations, *Adv. Space Res.*, *33*, 829–832.

Hughes, W. J., and D. J. Southwood (1976), An illustration of modification of geomagnetic pulsation structure by the ionosphere, *J. Geophys. Res.*, *81*, 3241–3247.

Jakowski, N., and M. Förster (1995), About the nature of the nighttime winter anomaly effect, *Planet. Space Sci.*, *43*, 603–612.

Kawano, H., K. Yumoto, V. A. Pilipenko, Y.-M. Tanaka, S. Takasaki, M. Iizima, and M. Seto (2002), Using two ground stations to identify magnetospheric field line eigenfrequency as a continuous function of ground latitude, *J. Geophys. Res.*, *107*(A8), 1202, doi:10.1029/2001JA000274.

Loto'aniu, T. M., C. L. Waters, B. J. Fraser, and J. C. Samson (1999), Plasma mass density in the plasmatrough: Comparison using ULF waves and CRRES, *Geophys. Res. Lett.*, *26*, 3277–3280.

McClay, J. F. (1970), On the resonant modes of a cavity and the dynamical properties of micropulsations, *Planet. Space Sci.*, *18*, 1673–1690.

Menk, F. W., D. Orr, M. A. Clilverd, A. J. Smith, C. L. Waters, D. K. Milling, and B. J. Fraser (1999), Monitoring spatial and temporal variations in the dayside plasmasphere using geomagnetic field line resonances, *J. Geophys. Res.*, *104*, 19,955–19,969.

Menk, F. W., C. L. Waters, and B. J. Fraser (2000), Field line resonances and waveguide modes at low latitudes: 1. Observations, *J. Geophys. Res.*, *105*, 7747–7761.

Menk, F. W., I. R. Mann, A. J. Smith, C. L. Waters, M. A. Clilverd, and D. K. Milling (2004), Monitoring the plasmapause using geomagnetic field line resonances, *J. Geophys. Res.*, *109*, A04216, doi:10.1029/2003JA010097.

Namgaladze, A. A., M. Förster, and R. Y. Yurik (2000), Analysis of the positive ionospheric response to a moderate geomagnetic storm using a global numerical model, *Ann. Geophys.*, *18*, 461–477.

Ozeke, L. G., and I. R. Mann (2005), High and low ionospheric conductivity standing guided Alfvén wave eigenfrequencies: A model for plasma density mapping, *J. Geophys. Res.*, *110*, A04215, doi:10.1029/2004JA010719.

Pilipenko, V. A., K. Yumoto, E. N. Fedorov, N. Kurneva, and F. W. Menk (1998), Field line Alfvén oscillations at low latitudes, *Earth Planet. Sci.*, *XXX*, 23–43.

Poulter, E. M., and W. Allan (1985), Transient ULF pulsation decay rates observed by ground based magnetometers: The contribution of spatial integration, *Planet. Space Sci.*, *33*, 607–616.

Poulter, E. M., W. Allan, G. J. Bailey, and R. J. Moffett (1984), On the diurnal period variation of mid-latitude ULF pulsations, *Planet. Space Sci.*, *32*, 727–734.

Poulter, E. M., W. Allan, and G. J. Bailey (1988), ULF pulsation eigenperiods within the plasmasphere, *Planet. Space Sci.*, *36*, 185–196.

Poulter, E. M., W. Allan, and G. J. Bailey (1990), The effect of density inhomogeneity on standing Alfven wave structure, *Planet. Space Sci.*, *38*, 665–673.

Price, I. A., C. L. Waters, F. W. Menk, G. J. Bailey, and B. J. Fraser (1999), A technique to investigate plasma mass density in the topside ionosphere using ULF waves, *J. Geophys. Res.*, *104*, 12,723–12,732.

Radoski, H. R. (1966), Magnetic toroidal resonances and vibrating field lines, *J. Geophys. Res.*, *71*, 1891–1893.

Reinisch, B. W., X. Huang, P. Song, G. S. Sales, S. F. Fung, J. L. Green, D. L. Gallagher, and V. M. Vasyliunas (2001), Plasma density distribution along the magnetospheric field: RPI observations from IMAGE, *Geophys. Res. Lett.*, *28*, 4521–4524.

Richards, P. G., et al. (2000), On the relative importance of convection and temperature on the behavior of the ionosphere in North America during January 6–12, 1997, *J. Geophys. Res.*, *105*, 12,763–12,776.

Russell, C. T., P. J. Chi, V. Angelopoulos, W. Goedecke, F. W. Chun, G. Le, M. B. Moldwin, and G. D. Reeves (1999), Comparison of three techniques for locating a resonating magnetic field line, *J. Atmos. Sol. Terr. Phys.*, *61*, 1289–1297.

Schulz, M. (1996), Eigenfrequencies of geomagnetic field lines and implications for plasma-density modeling, *J. Geophys. Res.*, *101*, 17,385–17,397.

Sutcliffe, P. R., S. K. F. Hattingh, and H. F. V. Boshoff (1987), Longitudinal effects on the eigenfrequencies of low-latitude Pc 3 pulsations, *J. Geophys. Res.*, *92*, 2535–2543.

Takahashi, K., and R. L. McPherron (1982), Harmonic structure of Pc 3–4 pulsations, *J. Geophys. Res.*, *87*, 1504–1516.

Takahashi, K., R. E. Denton, R. R. Anderson, and W. J. Hughes (2004), Frequencies of standing Alfvén wave harmonics and their implication for plasma mass distribution along geomagnetic field lines: Statistical analysis of CRRES data, *J. Geophys. Res.*, *109*, A08202, doi:10.1029/2003JA010345.

Taylor, J. P. H., and A. D. M. Walker (1984), Accurate approximate formulae for toroidal standing hydromagnetic oscillations in a dipolar geomagnetic field, *Planet. Space Sci.*, *32*, 1119–1124.

Tu, J.-N., J. L. Horwitz, P. Song, X.-Q. Huang, B. W. Reinisch, and P. G. Richards (2003), Simulating plasmaspheric field-aligned density profiles measured with IMAGE/RPI: Effects of plasmasphere refilling and ion heating, *J. Geophys. Res.*, *108*(A1), 1017, doi:10.1029/2002JA009468.

Vellante, M., U. Villante, M. De Lauretis, and G. Barchi (1996), Solar cycle variation of the dominant frequencies of Pc3 geomagnetic pulsations at L = 1.6, *Geophys. Res. Lett.*, *23*, 1505–1508.

Vellante, M., M. De Lauretis, M. Förster, S. Lepidi, B. Zieger, U. Villante, V. A. Pilipenko, and B. Zolesi (2002), Geomagnetic field line resonances at low latitudes: Pulsation event study of 16 August 1993, *J. Geophys. Res.*, *107*(A5), 1060, doi:10.1029/2001JA900123.

Vellante, M., et al. (2004), Ground/satellite signatures of field line resonance: A test of theoretical predictions, *J. Geophys. Res.*, *109*, A06210, doi:10.1029/2004JA010392.

Warner, M. R., and D. Orr (1979), Time of flight calculations for high latitude geomagnetic pulsations, *Planet. Space Sci.*, *27*, 679–689.

Waters, C. L., F. W. Menk, and B. J. Fraser (1991), The resonance structure of low latitude Pc3 geomagnetic pulsations, *Geophys. Res. Lett.*, *18*, 2293–2296.

Waters, C. L., F. W. Menk, and B. J. Fraser (1994), Low latitude geomagnetic field line resonance: Experiment and modeling, *J. Geophys. Res.*, *99*, 17,547–17,558.

Waters, C. L., J. C. Samson, and E. F. Donovan (1995), The temporal variation of the frequency of high latitude field line resonances, *J. Geophys. Res.*, *100*, 7987–7996.

Waters, C. L., J. C. Samson, and E. F. Donovan (1996), Variation of plasmatrough density derived from magnetospheric field line resonances, *J. Geophys. Res.*, *101*, 24,737–24,745.

Yumoto, K., V. A. Pilipenko, E. N. Fedorov, N. Kurneva, and K. Shiokawa (1995), The mechanisms of damping of geomagnetic pulsations, *J. Geomagn. Geoelectr.*, *47*, 163–176.

Zesta, E., A. Boudouridis, D. Berube, and M. B. Moldwin (2004), Conjugate observations of field-line resonances in the inner magnetosphere from the MEASURE and SAMBA magnetometer chains, paper presented at the 2004 Fall Meeting, AGU, San Francisco, Calif.

M. Förster, GeoForschungZentrum Potsdam, Division 2.3, Telegrafenberg, D-14473 Potsdam, Germany. (mfo@gfz-potsdam.de)

M. Vellante, Dipartimento di Fisica, Università dell'Aquila, Via Vetoio 10, I-67010 Coppito-L'Aquila, Italy. (massimo.vellante@aquila.infn.it)